Analysis of FSI effects for a novel WEC using high-fidelity simulations

Master's thesis in Applied Mechanics

Jason Ebenezer John Jawahar Edwin

Department of Mechanics and Maritime Sciences
CHALMERS UNIVERSITY OF TECHNOLOGY
Gothenburg, Sweden 2022
www.chalmers.se

Master's thesis 2022:39

Analysis of FSI effects for a novel WEC using high-fidelity simulations

JASON EBENEZER JOHN JAWAHAR EDWIN

Department of Mechanics and Maritime Sciences
Division of Marine Technology
Chalmers University of Technology
Gothenburg, Sweden 2022

Analysis of FSI effects for a novel WEC using high-fidelity simulations
JASON EBENEZER JOHN JAWAHAR EDWIN

Examiner: Jonas Rinsberg (jonas.ringsberg@chalmers.se)
Supervisor at Chalmers: Hua-Dong Yao (huadong@chalmers.se),
Supervisor at Chalmers: Xinyuan Shao (xinyuan.shao@chalmers.se)

Master's Thesis 2022:39
Department of Mechanics and Maritime Sciences
Division of Marine Technology
Chalmers University of Technology
SE-412 96 Gothenburg
Telephone +46 31 772 1000

Typeset in LaTeX
Printed by Chalmers Reproservice
Gothenburg, Sweden 2022

Analysis of FSI effects for a novel WEC using high-fidelity simulations
JASON EBENEZER JOHN JAWAHAR EDWIN
Department of Mechanics and Maritime Sciences
Chalmers University of Technology

Abstract

Wave energy is more reliable and continuous in time, compared to solar and wind energy which are more periodic. The World Energy Council predicts that wave energy has the potential to meet 10-20% of the world's energy demands. A wave energy converter (WEC) as the name suggests, harvests energy from the vertical motion of waves. The WEC is anchored in an offshore location, using mooring lines attached to the sea floor. The generated electricity is transmitted to a grid on-land, since the WEC does not have an energy storage system, to keep the weight of the WEC low. In this project, a WEC is studied using the commercial CFD code STAR-CCM+. The WEC is designed by Novige AB called NoviOcean 500. The primary objective is to study the forces acting on the surface of the buoy as a result of the heave, surge and pitch motions, which affect the power generation and the stability of the buoy in the waves. It is equally important to study the mooring line forces of the WEC, for design estimations of the mooring line material and size. A mesh independence study is done to ensure the results of the study are mesh independent. The different wave generation models, the fifth order Stokes wave and irregular wave models are considered, with the irregular wave model being found more suited for short sea states, like stormy sea conditions. And the fifth order Stokes wave more uniform and regular in nature. Various wave parameters which affect the heave motion of the WEC, like wavelength and wave period are studied. A nominal wave period between 5-9 seconds is used to depict normal sea wave conditions. Finally, the linear spring and catenary coupling models are used to study the differences in heave motion, coupling elongation and coupling forces. From the thesis work, it is concluded that the use of the fifth order Stokes wave model, with a wave period of between 5-9 seconds and a catenary coupling model for the mooring lines, is a good simulation setup for the study of the NoviOcean 500

Keywords: WEC, buoy, CFD, wave energy, mooring, overset mesh, fluid structure interaction

Acknowledgements

As the master's program draws to an end, I would like to reflect on my time at Chalmers University of Technology during the last two years, which has been an eventful and memorable one. I am thankful for the professors and friends, who have immensely helped me and having learnt so many things from them, I would always be grateful for their acquaintances.

Secondly, I would like to thank my supervisors at Chalmers University of Technology, Prof. Hua-Dong Yao and Xinyuan Shao for their help and support throughout the project duration. They have always encouraged and guided me throughout this time.

I would also like to specially thank my examiner at Chalmers University of Technology, Prof. Jonas Rinsberg for his valuable feedback and guidance through this project.

Finally, I would like to thank my parents for the support they have provided during my entire education and how they always been in my corner cheering for me.

Jason Ebenezer John Jawahar Edwin, Gothenburg, June 2022

Notations

Abbreviations

CAD	Computer Aided Design
CFD	Computational Fluid Dynamics
DFBI	Dynamic Fluid Body Interaction
DOF	Degree of Freedom
FSI	Fluid-Structure Interaction
NS	Navier-Stokes
PDE	Partial Differential Equation
PTO	Power Take Off
TWh	Terawatt-hour
VOF	Volume of Fluid
WEC	Wave Energy Converter

Greek symbols

λ	Wavelength
ρ	Density
σ	Stress tensor
τ	Viscous stress tensor
ω	Wave frequency

Roman symbols

f_b	Body force
f_i	Force component
H	Wave height
H_s	Significant wave height
k	Kinetic energy
K	Wave vector
k_{eff}	Elastic coefficient
q_i	Heat energy
T	Stress tensor
u	Internal energy
U_R	Ursell number

$\dot{x}$	Relative velocity between the end points
x_o	Relaxation length of spring

Contents

List of Figures

List of Tables

1

Introduction

1.1 Background

Ocean waves offer a lot of potential in the area of renewable and sustainable energy resources and offer a good alternative to many countries on the path of decarbonisation of their energy sources. Unlike solar and wind energy which are highly dependent on seasons and other factors, wave energy is available throughout the year. It can be mentioned that for the same surface area, the extractable energy from waves is about 4 times more than wind power and 20 times more than solar cells. Another advantage is that it also does not occupy real estate on land, since these instruments are deployed in the oceans. Furthermore, the potential annual global production is estimated at 29,500 TWh. This is almost ten times Europe's annual electricity consumption of 3,000 TWh [1].
The wave energy converter (WEC) NoviOcean 500 has a buoy whose general shape is rectangular, with a curved profile on the side facing the oncoming waves. The unit is shown in Figure 2.6. NoviOcean 500 is deployed at a water depth of 50-60 meters. The mooring lines are anchored to the sea-bed to hold the buoy in position. NoivOcean 500, is a point-absorber type of WEC, which harvests wave energy at the surface of the sea. The WEC converts the kinetic energy in the waves to useful electrical energy, through a PTO unit place on-board the unit. For this reason, the various forces acting on the WEC and the behaviour of the WEC are important in predicting the power generation and survivability under different weather conditions and mooring line requirements.

1.2 Problem statement

With growing interest in wave energy and the clear potential of wave energy [1] to meet the world's energy demands, wave energy is not being fully utilized. Due to two major drawbacks: one is the nascent stage of development of the technology and second the high costs of production of wave energy compared to other green and renewable energy alternatives available [2]. While 70% of our earth is covered with water, of which only 0.02% of that is all the lakes and rivers, it still accounts for a quarter of world energy needs to be met. The potential with wave energy is high and can be tapped into, by addressing the above two points working against it. In NoviOcean 500, both points are being addressed by using a patented PTO system concept, similar to the systems used in hydro-electric power generation and having operating and total costs below the industry median [3]. The main objective of this thesis includes studying the FSI of the WEC with the waves for various parameters, using the commercial CFD code STAR-CCM+. These objectives include the determination of the optimal wavelength and wave period parameters, optimal wave generation model, coupling models that accurately depict mooring line behaviour and the resultant effects on the heave motion of NoviOcean 500.

1.3 Limitations

STAR-CCM+ is used to consider and simulate many non-linear effects, but not that of the mooring lines. STAR-CCM+ uses a simplified linear-theory for determination of mooring line forces rather than non-linear theories, which are considered more accurate. As a future step in the study, this simplification can be addressed by using a dedicated tool like SESAM for mooring line forces calculation, which can be integrated with STAR-CCM+.

1.4 Thesis aims and layout

The aim of the thesis is to setup, simulate and study the results of the WEC interacting with the waves for various parameters like wave height, wave time-period, wavelength, water depth along with various coupling models like spring-damper and catenary models.
The layout of the thesis is as follows:

- Chapter 2 presents about the physics of the simulation, the various types of WEC's available, the working theory of NoviOcean 500 and the coupling systems used in the thesis.
- Chapter 3 gives an overview about the method of modelling NoviOcean 500 geometry and mesh strategy used in the thesis.
- Chapter 4 contains the mesh independence study, various wave models studied, coupling models for the mooring lines and other wave propagation parameters. The results of these studies are presented and discussed in the chapter.
- Chapter 5 gives the conclusion of this thesis and some perspectives for future studies.

2
Theory

In this chapter, the theories relating to the wave generation model, force coupling systems, type of WEC are discussed in detail to give the reader an understanding. Also an overall view on the flow governing equations is also discussed to give insight.

2.1 Flow governing equations

The three main governing equations that govern any fluid flow are the continuity equation, the momentum equation and the energy equation. These equations signify the fundamental physics of any problem and state the conservation of mass, momentum and energy respectively. In any CFD problem, these equations have to be solved to obtain the flow field.

2.1.1 The continuity equation

In fluid mechanics, the continuity equation states that the volume of fluid in a space is affected by only the volume of fluid that flows in and out of that volume. The 'law of conservation of mass' states that mass can be neither created nor destroyed [4].

For an incompressible flow (ρ = constant) [4], it is:

$$\frac{\partial v_i}{\partial x_i} = 0 \tag{2.1}$$

2.1.2 The momentum equation

The second governing equation is the momentum equation, which is based on the Newton's second law of motion, which states when a body is acted upon by a force, the time rate of change of its momentum equals the force acting on it. It can be expressed as below:

$$\rho \frac{dv_i}{dt} = \frac{\partial \sigma_{ji}}{\partial x_j} + \rho f_i$$

where the term $\frac{\partial \sigma_{ji}}{\partial x_j}$ denotes the net force due to surface force (σ_{ji} is the stress tensor), which also includes the viscous stress tensor (τ_{ij}) and the term ρf_i denotes volume force. Further, substituting $\sigma_{ij} = -\frac{\partial P}{\partial x_i} + \mu \frac{\partial^2 v_i}{\partial x_j \partial x_j}$ in the above equation, for an incompressible flow, we get the below equation, which is also called the "Navier-Stokes equation"[4]:

$$\rho \frac{dv_i}{dt} = -\frac{\partial P}{\partial x_i} + \mu \frac{\partial^2 v_i}{\partial x_j \partial x_j} + \rho f_i \tag{2.2}$$

2.1.3 The energy equation

The third governing equation with fluid dynamics is the energy equation, which is concerned with the conservation of energy, is based on the first law of thermodynamics. This law can be summarized as that "the rate of change of energy in a system is equal to the sum of net flux of heat into the system and rate of work done, i.e., energy can neither be created nor destroyed" [4]. The energy equation is defined as:

$$\rho \frac{d(u+k)}{dt} = \frac{\partial \sigma_{ji} v_i}{\partial x_j} - \frac{\partial q_i}{\partial x_i} + \rho v_i f_i \tag{2.3}$$

This equation denotes the sum of internal (u) and kinetic (k) energies. And q_i denotes the heat energy [4].

Since in the thesis only laminar flow has been assumed and no turbulence is considered, the above discussed governing equations are sufficient to solve the flow field and no turbulence modelling is needed.

2.2 Volume of Fluid (VOF)

Since the thesis involves a multi-phase problem (air and water), this section talks briefly about the physics behind solving a multi-phase problem. The VOF model is used to simulate flows of several immiscible fluids on a regular and stationary grid which are capable of solving the interface between the two phases of the mixture [10]. Further a phase indicator function is used to indicate the fractional amount of fluid at a certain position. This method suits this study, since there is only a small contact area between the phases (at the water surface). Also the free surface remains relatively smooth, without much breaking of the water resulting in many water droplets in the air, which then requires a too fine grid setup.
The governing equations mentioned under the previous section are now applied to the multi-phase fluids and the continuity and the momentum equation are expressed below [10]:

$$\frac{\partial \rho}{\partial t} + \nabla .F.(\rho u) = 0 \tag{2.4}$$

$$\frac{\partial}{\partial t}(\rho u) + \nabla .F.(\rho u u) = -\nabla p I + \nabla .F.T + \rho g + f_b \tag{2.5}$$

where p is the pressure, I is the unity tensor, T is the stress tensor, f_b is the vector of body forces.

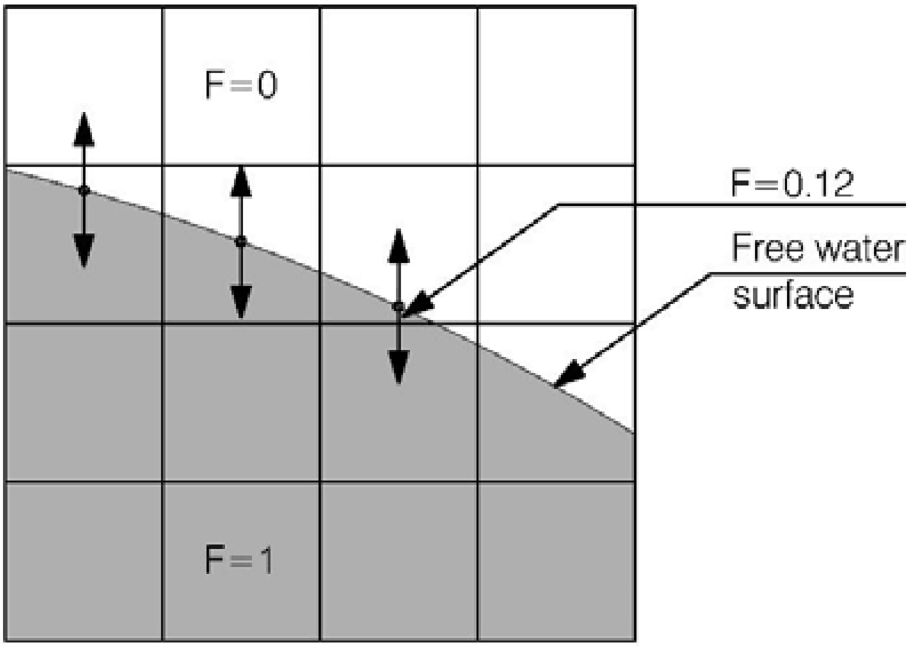

Figure 2.1: VOF grid representation, F is the phase-indicator function [13].

2.3 Wave energy

Under this section, the most commonly used methods of wave energy generation are discussed, to give the reader a brief insight into this field. Further towards the end, a section discussing NoviOcean 500 WEC is also included.

Wave energy is a form of renewable energy that can be harnessed from the kinetic motion of the waves. The waves itself are generated as a result of different lunar cycles and wind patterns, which determine the wave height, wavelength, wave speed and wave density. The kinetic energy from these waves can be harnessed through various devices that are placed either at the surface or submerged in a ocean and can be used to generate useful mechanical or electrical energy called a wave energy converter (WEC).

Though wave energy is considered to have the biggest potential among all renewable sources of energy, it is often constrained by the wave characteristics at different parts of the world. For example, the coasts of Norway are 10 times more energy dense than the coasts of Sweden for wave energy. The Figure 2.2 is a energy density map for wave energy, which shows the potential for wave energy harnessing.

2.3.1 Wave Energy Converter (WEC)

There are various types of WEC, a few examples of the various designs are introduced in this section and discussed briefly with respect to their working designs.

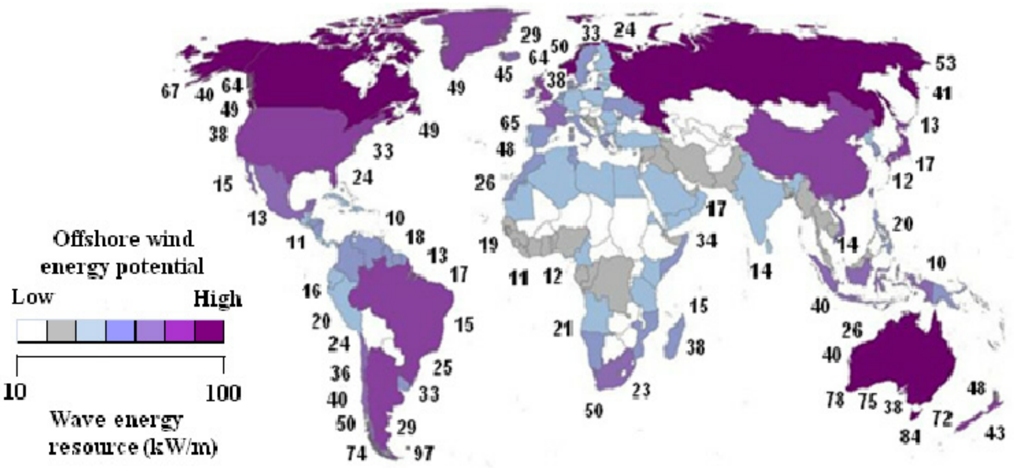

Figure 2.2: Global distribution of offshore wind and wave energy resources. Wave energy density is denoted by the number scale [5].

2.3.1.1 Point type wave absorber

The point type wave absorber is a surface-type absorber that harvests kinetic energy contained from the vertical motion (heave) of waves. In this type of WEC, the upper end is floating at the surface and moves freely with the wave motion, and the lower end is usually fixed to the sea-bed, as shown using the below figure.

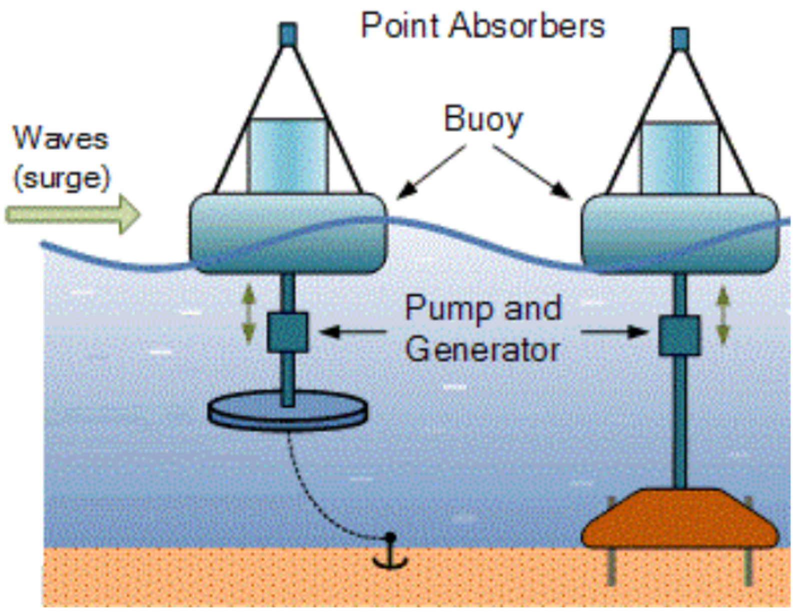

Figure 2.3: Design layout of point type absorber [7].

2.3.1.2 Oscillating water column

The oscillating water column type WEC has a water column with air in it's chamber. As the water level rises during the crest of the wave, this compresses the air inside the column. The pressurized air is then forced to exit through a small passage containing the turbine generating electricity. A schematic layout of such a WEC is shown in the below Figure 2.4.

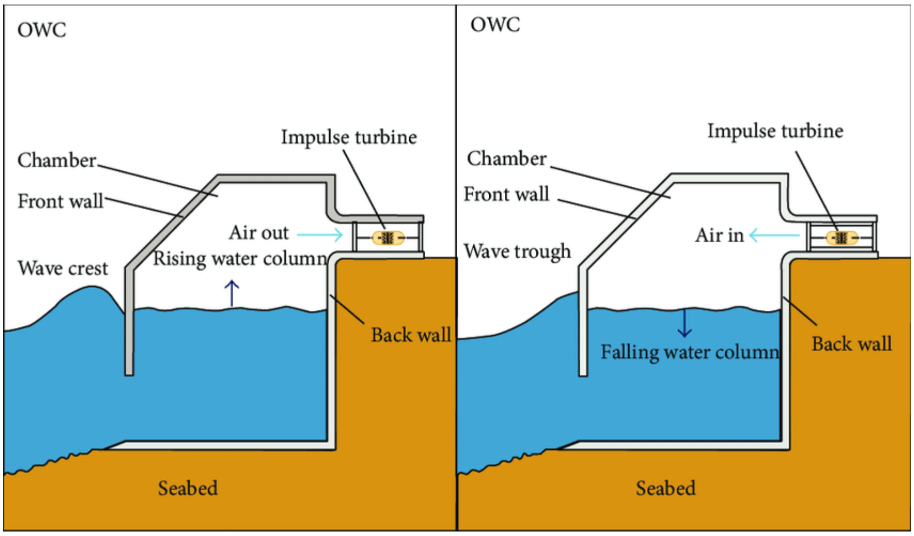

Figure 2.4: Design layout of an oscillating water column [8].

2.3.1.3 Attenuators

This type of WEC is placed in a direction that is perpendicular to the direction of the waves, and generates electricity through the flexing of the joints.

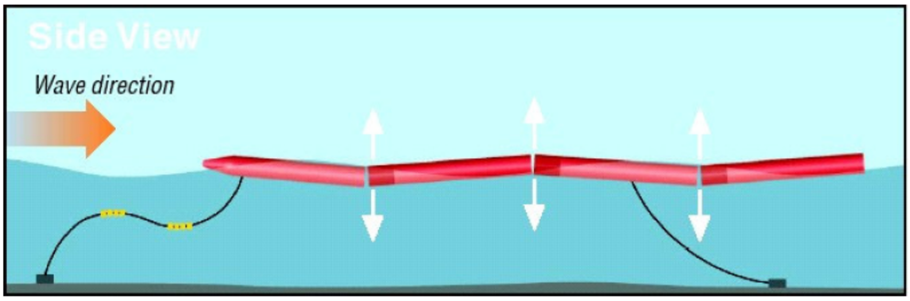

Figure 2.5: Attenuator setup [9].

2.3.2 NoviOcean 500

Now the WEC in this study is NoviOcean 500, which fundamentally works with the same concept as the point-type WEC discussed in the previous section. The clear advantages of this type of WEC, is that there is no permanent structure, as in the oscillating water column. And the NoviOcean 500 can orient itself to face the waves headlong, thereby always harvesting full potential of wave energy. The disadvantages of such a design is the survivability of the WEC in severe sea states and size of the PTO unit on the top, which is limited by size of the buoy.

The upper end of the WEC is floating on the sea-surface, as can be seen in the Figure 2.6. The lower end is fixed to the sea floor, as seen in the simple sketch depicting NoviOcean 500 in Figure 2.7. The lower part of the WEC which is partially submerged on the water surface moves vertically with the heave motion of the oncoming waves, the base of the WEC is fixed to the sea-bed. Sea water fills the tube structure which is being compressed due to the heave motion of the WEC. The compressed sea water is then sent to the inverted PTO unit which is placed at the top of the WEC (see in Figure 2.6), from the cylinder in the bottom. This pressurized water is used to drive a turbine and generate electricity. So with each incoming wave, the WEC rises and falls along with the waves to compress water, which is then converted to usable energy resource.

Figure 2.6: NoviOcean 500 scale prototype, source: Novige AB.

2.4 Wave generation model

This section gives the reader an overview about the wave-generation model theory that is being used in STAR-CCM+ to generate and simulate waves.

2.4.1 Fifth-order Stokes wave model

Fifth order Stokes waves are modeled using the fifth order approximation for the Stokes theory of waves. The theory is valid for large wavelengths and intermediate to deep water depths [14]. Wavelength is defined as the distance between two successive crests or troughs. The fifth order Stokes wave model is used in comparison to the other available models like first order waves, cnoidal waves, irregular waves, because of its closer resemblance to actual physical waves [10]. The wave profile and velocity are given based on parameters like water depth, wave height. An non-dimensional number called the Ursell number (Stokes parameter) is used to check the valid use of the wave theory to the defined parameters. It is defined as:

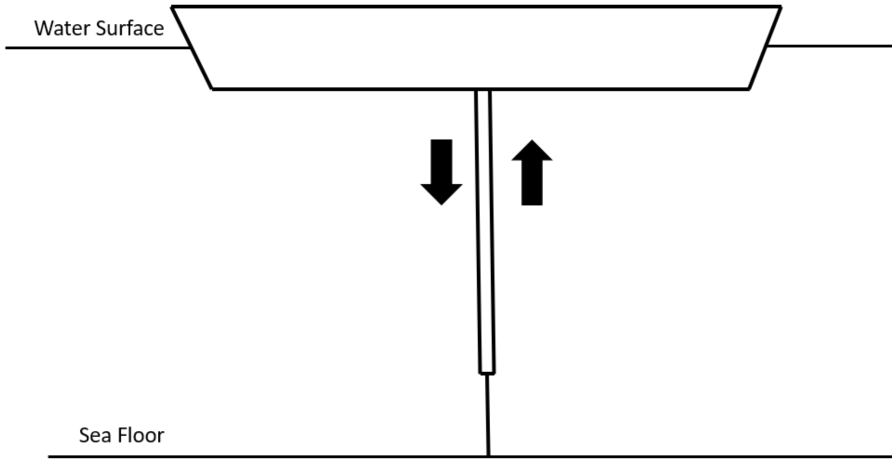

Figure 2.7: NoviOcean 500 simple sketch, Side view.

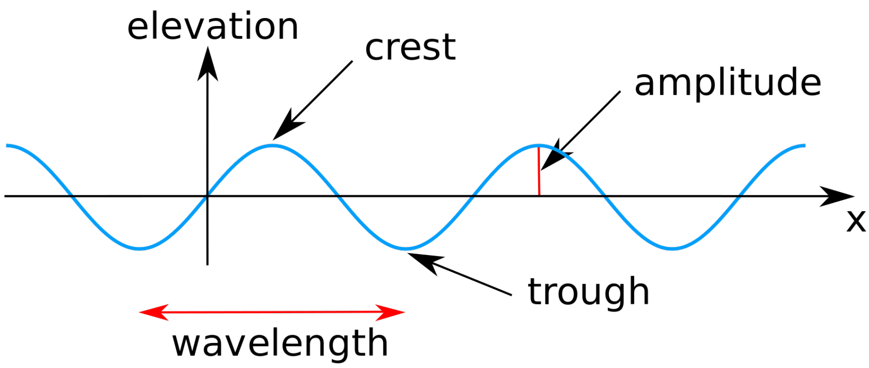

Figure 2.8: Wave characteristics [11].

$$U_R = \frac{H\lambda^2}{d^3}$$

where H is the wave height, λ is the wavelength and d is the water depth. For values of Ursell number below 30, the fifth-order Stokes wave model can be used accurately [10].

2.4.2 Irregular wave model

An irregular wave model is used to model wind seas (a short-term sea state) with a wave spectrum, that is, the power spectral density function of the vertical sea surface displacement. Here the Pierson-Moskowitz spectrum is used. This spectrum describes the wind sea conditions that occur for severe sea states [10].

$$S_{PM}(\omega) = \frac{5}{16}(H_S^2\omega_p^4)\omega^{-5}exp(\frac{-5}{4}(\frac{\omega}{\omega_p})^{-4})$$

where $\omega_p = \frac{2\pi}{T_P}$ represents the angular spectral frequency.
This wave model is used to study severe sea states, similar to those occurring during storms.

2.5 Body Couplings

The WEC in the simulation setup is assigned as the Dynamic Fluid Body Interaction (DFBI) since the WEC moves with the waves and is not stationary in the simulation. This option enables to solves all 6 DOF motion associated with the body. Since the WEC is anchored to a certain location using mooring (anchor) lines, it is important to simulate such mooring line forces as part of the simulation. For this reason, body couplings, to model an actual mooring line are used. These are the spring-damper coupling and the catenary coupling, which are discussed in brief in the below sections.

2.5.1 Spring-Damper coupling

As the name suggests, this coupling element models a realistic spring between the WEC and the environment, where a damping force is applied through the spring. This damping force ensures that a force is applied to the WEC, that keeps its position relatively constant [10] [18]. One end of the spring is fixed at a position close to the center of the buoy and about one-third of the distance from the bottom of the WEC. And the other end is fixed in the environment. A relaxation length is set, to ensure that no spring force is exerted on the WEC at this length.

2.5.2 Catenary coupling

This coupling element, which maybe more closely represents the mooring lines, models a quasi-stationary, elastic catenary (a curve formed by a wire, rope, or chain hanging freely from two points that are not in the same vertical line) between the WEC and the environment as shown in the below Figure 2.9. The catenary relaxation length (at which no force is applied) or the pretension force are defined in the simulation.

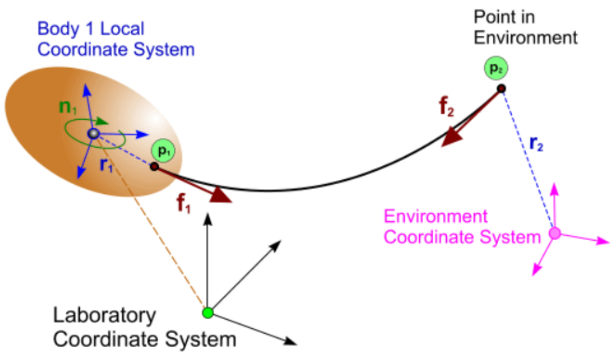

,

Figure 2.9: Catenary coupling schematic between a body and the environment [10].

3
Methodology

Under this chapter, the methods used in this project are discussed, which includes the modeling of the geometry using CATIA V5, the mesh strategy used for the simulation setup.

3.1 Modeling of geometry

The modelling of the buoy geometry was done using CATIA V5, using the surface modelling options. The CAD model was provided and the modeling was done based on the given dimensions. Below Figures 3.2 and 3.1 are drawings of the WEC, to understand the dimensions and profile. Figure 3.3 shows the modeled geometry using CATIA V5, with the cylinder included. If we refer to Figure 2.6 on the prototype model, it can be seen that the inverted PTO unit at the top is not included in this simulation to simplify the design. But the weight of the PTO is included in the overall weight of the WEC which is 150 tons.

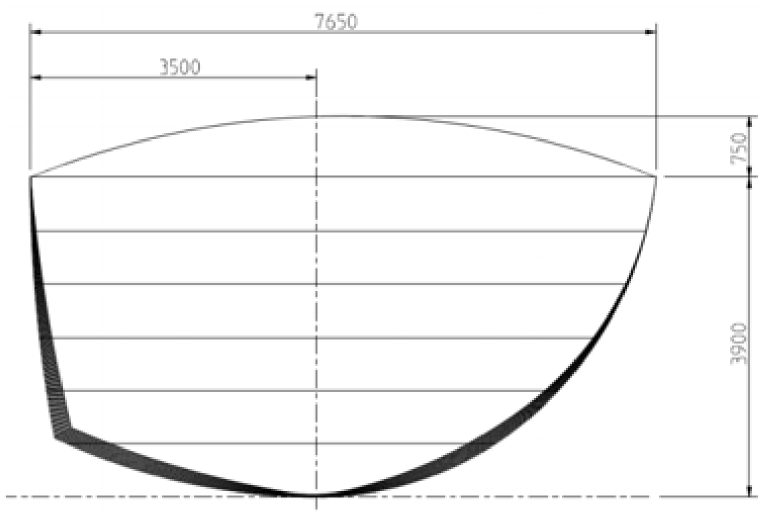

Figure 3.1: Geometry of NoviOcean500, Side profile. All dimensions in mm.

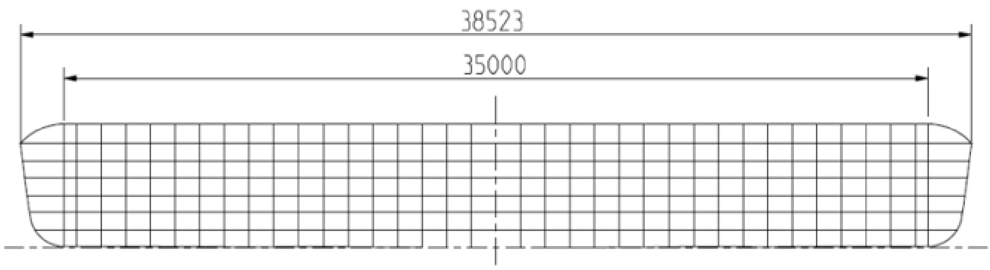

Figure 3.2: Geometry of NoviOcean500, Front view. All dimensions in mm.

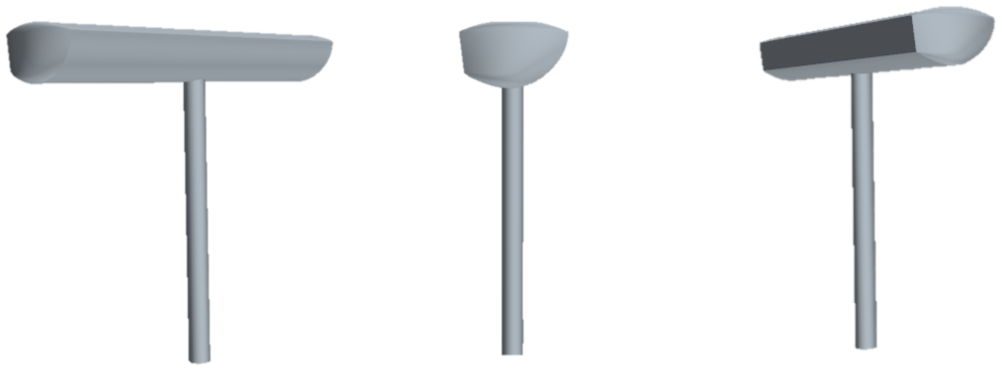

Figure 3.3: Modeled geometry using CATIA V5

In Figure 3.3, the first view on the left represents the side of the WEC that would be placed facing the waves, the curved profile helps the WEC to have a high wetted area and thereby harvest more kinetic energy from the waves.

3.2 Mesh strategy

The mesh strategy used here is the overset mesh in STAR-CCM+, since the body is in dynamic motion and transient with the waves [14][15]. The overset mesh is a meshing strategy where there is a secondary meshing region created around the moving body (in this case the WEC) and over the background meshing region. This overset mesh region moves relative to the body motion and information is transferred between the background and the overset region. This information transfer happens through what are called acceptor cells which act as the interface between the background and overset mesh regions. In these locations, seen in Figure 3.4, the mesh density difference between the background and oveset region must not be high, as this can lead to the solution divergence. The mesh refinement regions were done by using region based meshing and by creating parts in the domain to represent the various meshing regions, which then are controlled using volumetric mesh control.
The wave refinement region exists to capture the wave propagation characteristics, as per STAR-CCM+ recommendation [10] of 30-50 cells height-wise and 50-100 cells

span-wise. The ’Extruded region’ of the domain is where a wave-damping force is used to dampen the incoming waves into this region. This is done with the view to prevent the reflection effects of the wave on the WEC and to keep the computational domain small.

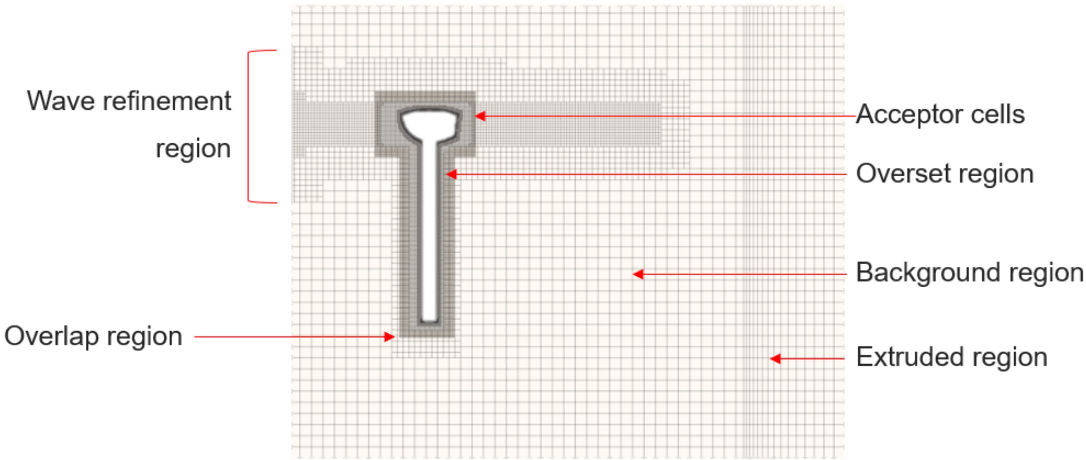

Figure 3.4: Overset mesh strategy, side view.

3.3 Interested results

In this section, the interest in the results to be analyzed further in the next chapter are discussed. The WEC has 6-DOF motions as shown in Figure 3.5, but the most important and central focus of this study is the ’heave motion’ which is in the vertical direction (z-axis). Since, this motion has direct correlation to the power generated by the NoviOcean 500 in different sea waves. An heave motion plot monitor is setup in STAR-CCM+ for every simulation, to monitor the relative motion of the WEC with respect to the initial water surface. The heave monitor plot helps us further understand the interaction effects of the NoviOcean 500 with the incoming waves.

Further, when using coupling models as part of the simulation. It is interesting to study the coupling elongation lengths and forces. As this helps in understanding the stresses of the coupling link as function of the stiffness and damping values and also to compare the behaviour of the different coupling systems available in STAR-CCM+. These results are of particular interest, since the focus of the study is to study the non-linear effects of hydrodynamic forces and motion acting on the WEC due to the motion of waves. STAR-CCM+ contains various wave generation models which closely depict the actual sea wave conditions. Also the tool SESAM is more focused on structural analysis of the WEC, which is useful when focusing on mooring line forces in particular.

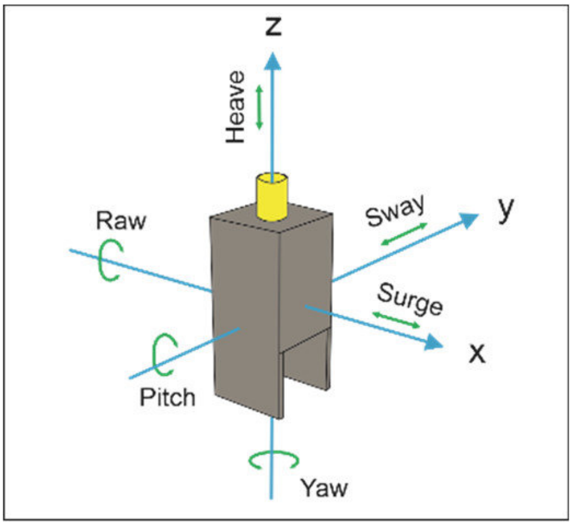

Figure 3.5: WEC various DOF's of motion [19].

4
Results and Discussion

4.1 Mesh independence study

The first section in the chapter discusses about validation of the mesh strategy used. This mesh dependence study was carried out by using only 1-DOF of motion for the WEC and no body couplings were used. The objective of the study was to understand the dependence of the results on the mesh size and to have a mesh strategy that was accurate and computationally efficient as well.

4.1.1 Simulation setup

First the configuration of the computational domain is discussed as shown in Figure 4.1. The domain is sized based on the parameter of wavelength. The wave originates from the velocity inlet boundary condition and propagates towards the pressure outlet. The streamwise distance before the WEC from the velocity inlet is recommended to be of 2 times wavelength. The streamwise distance after the WEC is taken as 4 times wavelength, which is again STAR-CCM+ recommendation [10]. The region of wave-damping is 2 times wavelength, where the incoming waves into this region are damped by a force to prevent wave reflection. The depth of the domain is around 60 m from the free surface. Also, the colour difference indicates the different phases present in the domain, where the region represented in red is air and the region represented in blue is water.
The boundary conditions are defined as velocity inlet on the right face and pressure outlet on the left face, as illustrated in Figure 4.1. The lower boundary is specified as sea-floor is wall, with no-slip boundary condition. The upper and side-boundaries are also specified as velocity inlet boundary condition[14] [16].

4.1.2 Results

The results are discussed on the basis of the value of heave motion measured on the body for the different mesh sizes, since this is the focus of the study. The mesh study was undertaken for mesh sizes ranging from 7.1 million total cell count to 1.8 million total cell count and classified as below with the number of cells. Note, that during the change in the overall mesh sizes, the ratio of difference in the number of cells in the background and overset mesh regions were kept close to constant to avoid divergence in the results.
These values of the study are summarized in Table 4.2. The heave motion at certain physical time milestones are taken from each mesh size and compared. The heave

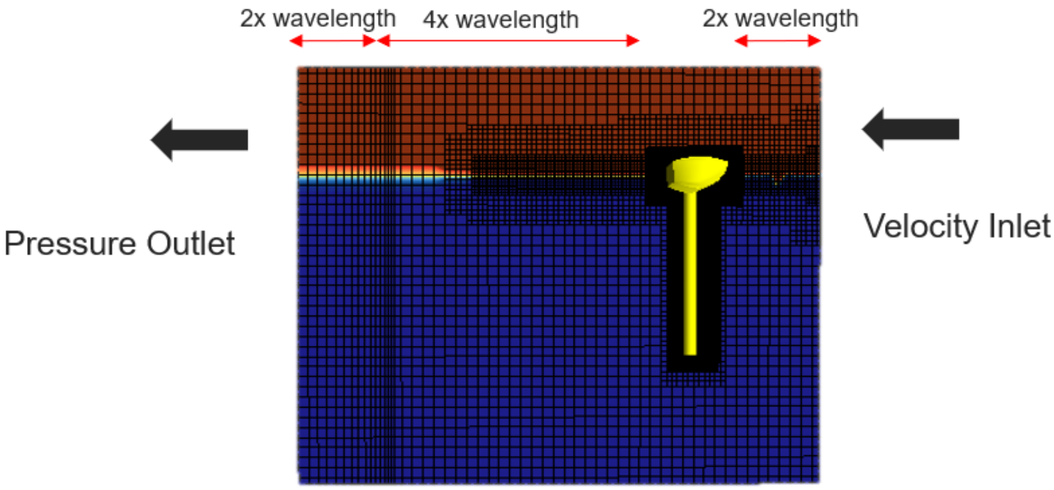

Figure 4.1: Computational domain 2D.

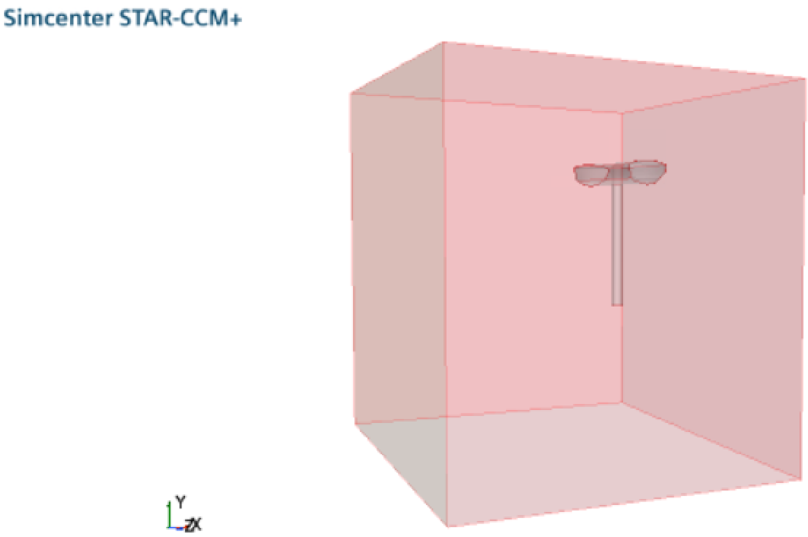

Figure 4.2: Computational domain configuration.

Table 4.1: Mesh independence study, mesh sizes.

Parameter	No of cells
Mesh strategy A	7,153,456
Mesh strategy B	3,796,853
Mesh strategy C	1,882,728

motion data of mesh strategy C was compared with the results of mesh strategy B. The percentage of difference between these two mesh strategies are summarized in the last column of the table, to show that the variance in the heave motion values is acceptable and the results are mesh independent.

In Figure 4.3, a graph showing the heave motion plots for the various mesh strategies

Table 4.2: Mesh independence study result summarized.

	Heave motion (m)			**% of change b/w (B) and (C)**
Physical time (s)	**Mesh strategy A**	**Mesh strategy B**	**Mesh strategy C**	
5	1.2606	1.34634	1.33248	-1.02
10	1.0661	1.13409	1.15835	2.14
15	0.99441	1.00778	1.01745	0.95
20	1.27182	1.29427	1.30006	0.47

are shown. The initial jump in the heave plot is not physical and is observed as a result of the first wave interacting with the WEC. But as it is observed as the physical time mature, there is a close agreement in the values of heave motion of mesh strategy B and strategy C.

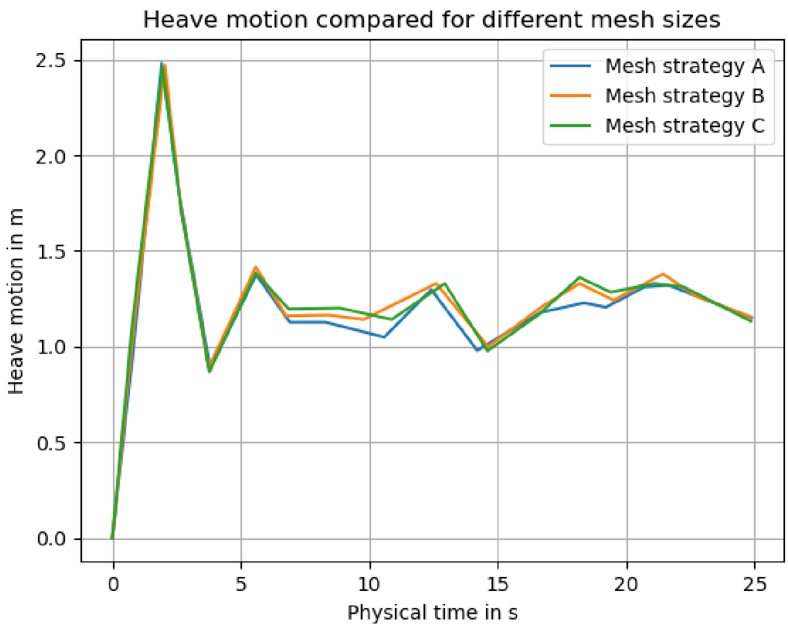

Figure 4.3: Comparison of heave plots between the different mesh strategies.

Based on the this study, the mesh strategy C is chosen for all the further simulations used in this project.

4.2 Irregular and fifth order Stokes waves

4.2.1 Simulation setup

In this section, the differences between the two wave-generation models which are closest to the physical world are compared. An irregular wave models wind seas with a wave spectrum, that is, the power spectral density function of the vertical sea surface displacement. In this case the Pierson-Moskowitz spectrum is used. This spectra describe wind sea conditions that often occur for the most severe sea states [10]. Now for the irregular waves, the significant wave height (H_s) is mentioned as 1.75 m and the peak wave period as 5 s. The significant wave height definition differs from the wave height definition in the fifth order Stokes wave model, in that it is the average height of the highest one-third waves [10].

4.2.2 Results

In Figure 4.5 the irregular wave state at a physical time of 25 s is shown, this is compared with the fifth order Stokes wave model heave motion shown in Figure 4.7. As it can be seen , the heave plot of the irregular wave model is very erratic and this is understandable, since this model is particularly used for predicting and simulating rough sea conditions [10]. This is in contrast with the fifth order Stokes model, which has a very periodic and uniform sine wave, in the heave motion plot shown in Figure 4.7. Further talking about the heave amplitude, it is observed that the fifth order Stokes model has a more uniform heave amplitude of around 2 m at the wave crest, in contrast to the irregular wave model. The irregular wave model has erratic heave amplitudes ranging from 1-2 m at the wave crest. Further, the wave periods observed for a simulation time of 25 s is not uniform for the irregular waves and is more periodic and uniform for the fifth order Stokes wave. Therefore, for all simulation settings used further in this project, the wave propagation model used is the fifth order Stokes wave model, since the focus of the study is the performance of NoviOcean 500 in regular sea-conditions.

Figure 4.4: Water surface for Irregular waves at simulation time, t=25 s.

4.3 Wavelength and wave period

4.3.1 Simulation setup

The Figure 4.8 shows the co-relation between significant wave height (H_s)(along the vertical axis) and the corresponding wavelength (along the horizontal axis). This is called a scatter plot or graph, which using the Cartesian coordinates displays the

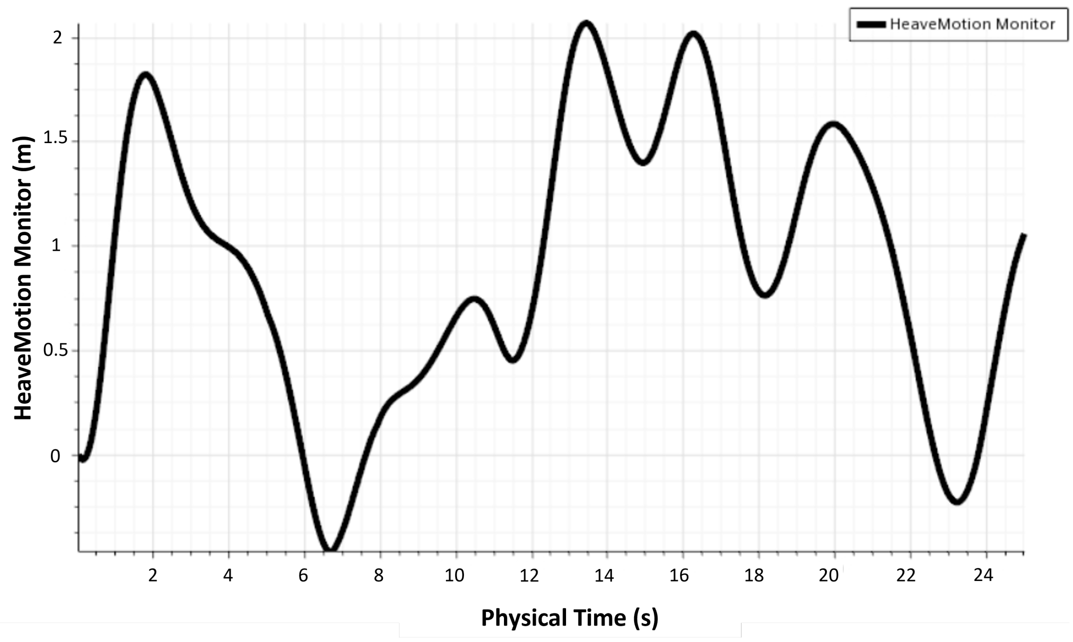

Figure 4.5: Heave plot for Irregular waves at simulation time, t=25 s.

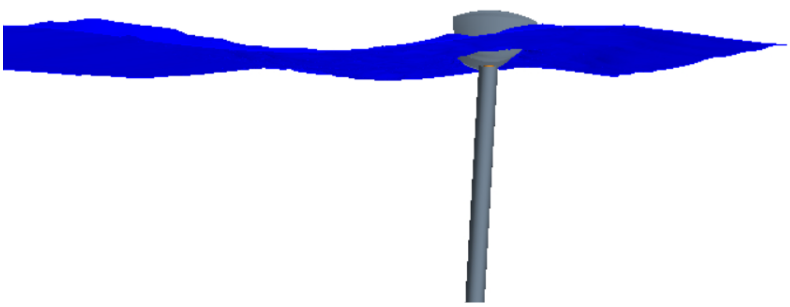

Figure 4.6: Water surface for fifth order Stokes wave at simulation time, t=25 s.

values for two variables for a set of data, which in this case is from one of the test sites of NoviOcean 500. The corresponding value in the table signifies the index for power generation capability for various co-relations and as it can be seen that for a H_s = 1.75 m and wavelength of 7.5 m, that the index is maximum, meaning these conditions are now used as parameters for the simulation setup. Since, the WEC's are not too far from the shore, the water depth is in the range of 50-60 m. And for these simulations, water depth is taken as 50 m and the wave height is 1.75 m as deduced from the scatter plot data.
The Table 4.3 shows the difference in wavelength and wave period for two cases, which will be discussed under this section. In case 1, the wavelength (λ) is specified

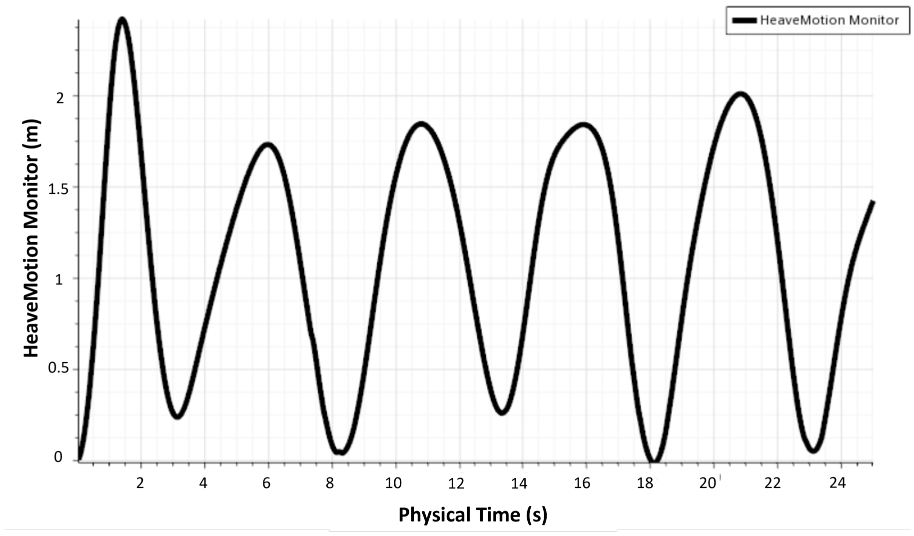

Figure 4.7: Heave plot for fifth order Stokes wave at simulation time, t=25 s.

Site Name	Bi-variate Frequency Scatter Plots																
	Sum	0	0	21.3	178.2	347	274.3	115	45.3	12.5	2.2	1	1.2	0.7	0.5	0	0
West of San Francisco, CA	Hm0/Te	2.5	3.5	4.5	5.5	6.5	7.5	8.5	9.5	10.5	11.5	12.5	13.5	14.5	15.5	16.5	17.5
	0.25				0												
	0.75				1	7	16	29	28	18	13	11	3	0			
	1.25			0	9	30	58	48	41	22	13	3	1	1	1	0	
	1.75				11	33	70	49	43	29	28	14	5	2	1	1	
	2.25				2	26	48	31	27	25	9	6	3	4	1	1	
	2.75					7	30	16	11	13	9	5	3	1	1	1	0
	3.25					2	14	6	6	7	6	3	1	0	0	0	0
	3.75					0	7	6	2	2	2	1	2		1	0	
	4.25						1	3	1	0	1		0	1		0	
	4.75						0	1	1	1				1	0		
	5.25							0		1				0	0		
	5.75																
	6.25																
	6.75																
	7.25																
	7.75																
	8.25																
	8.75																
	9.25																
	9.75																

Figure 4.8: Wave scatter data, source: Novige AB.

based on the scatter diagram as 7.5 m. Since, STAR-CCM+ allows the wave characteristics to be based upon the definition of only one parameter, which is either wavelength specification or wave period specification. So, when the wavelength was specified the wave period is calculated by default. The below equations define the calculation methodology used in STAR-CCM+.
The wave period T is defined as:

$$T = \frac{2\pi}{\omega}$$

where ω is the wave frequency The wavelength (λ) is defined as:

$$\lambda = \frac{2\pi}{K}$$

where K is the magnitude of wave vector[10]

Table 4.3: Wavelength and wave period

Case	Water depth (m)	Wavelength (m)	Wave period (s)
1	**50**	**7.5**	**1.68s**
2		**88.02**	**7.5**

4.3.2 Results

Based on the discussion in the previous section of the chapter, it can be understood that the wave period is calculated by default when the wavelength is specified and vice-versa. For case 1 as in Table 4.3, with wavelength of 7.5 m, the time-period of 1.68 s calculated by STAR-CCM+ is too small and non-physical. This means the WEC does not effectively interact with the heave motion of the waves, as can be seen from the heave plot for this case in Figure 4.9. Since the waves are too quick to interact with the WEC, before the WEC moves with the crest of the wave, the heave motion of the WEC is relatively flat throughout the physical time of simulation.

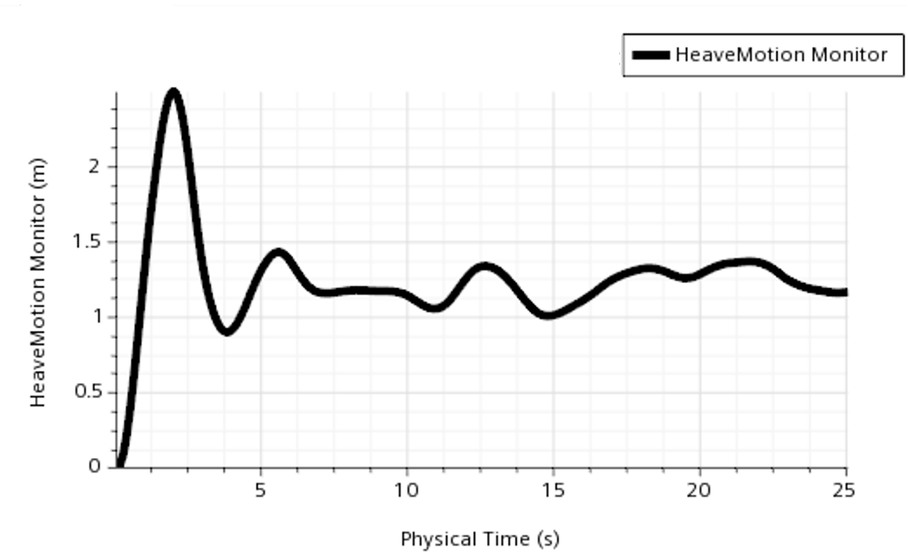

Figure 4.9: Heave plot diagram for case 1 at simulation time t=25 s, see Table 4.3.

So, a wave period close to 5-9 s which is desirable since it is more physical in nature is chosen for case 2. The wave period is then set at 7.5 s, which is the time between two successive crests or troughs to interact with the WEC. And the wavelength, though not physical is calculated by STAR-CCM+ to be 88.02 m as seen from Table 4.3. When the results are seen and compared with case 1, the case 2 results are more realistic and close to the expected result, with more periodic heave motions resembling the crests and troughs of the waves.

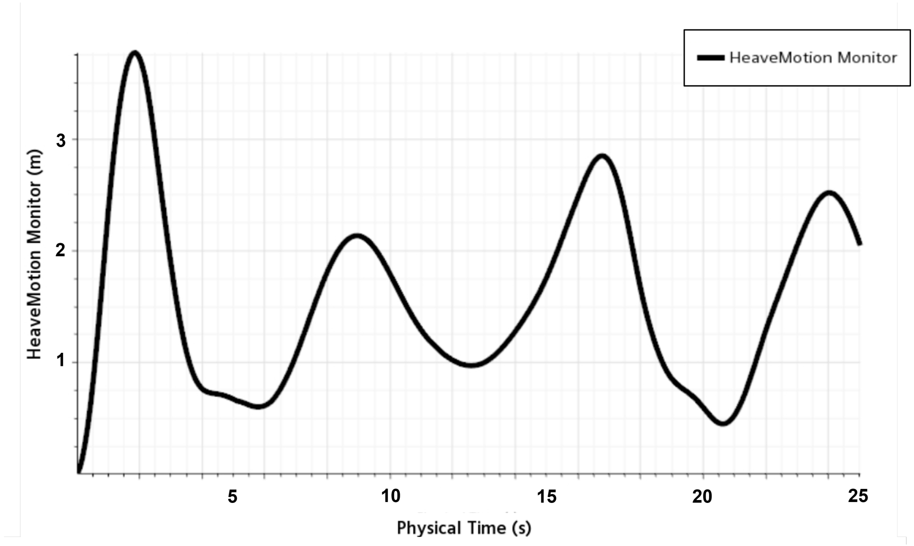

Figure 4.10: Heave plot diagram for case 2 at simulation time t=25 s, see Table 4.3

4.4 Coupling models

4.4.1 Without coupling and with coupling

In this section, the results with damping force applied and without damping are compared. As it can be seen from Figure 4.12 the difference is that only 1 DOF motion is enabled for the without coupling simulation setup and for the linear spring simulation, all 6 DOF's is enabled. This is in contrast to Figure 4.14 where the linear spring coupling is enabled and hence a damping force is being applied on the WEC. The difference can be seen in the heave motion plots for both the cases, where the case without coupling has higher heave motion values compared to the case with coupling, which have slightly lower heave motion values. This is expected because of the damping force applied on the WEC by the linear spring system.
The elastic and damping coefficients are defined as given in Table 4.4, for the linear spring coupling system. The elastic and damping forces based on the coefficients are summed up to give the force acting on the first end of the position vector and the equal and opposite force is applied on the second end of the position vector.

$$f_1(x) = k_{eff}(x - x_o) + k_d\dot{x}$$

$$f_2(x) = -f_1(x)$$

x is the scalar distance between the two end points, x_o is the relaxation length of the spring (at which elastic force vanishes), k_{eff} is the elastic coefficient, k_d is the damping coefficient, $\dot{x}$ is the relative velocity between the two end points of the system.

Figure 4.11: Water surface without damping force at simulation time, t=50 s.

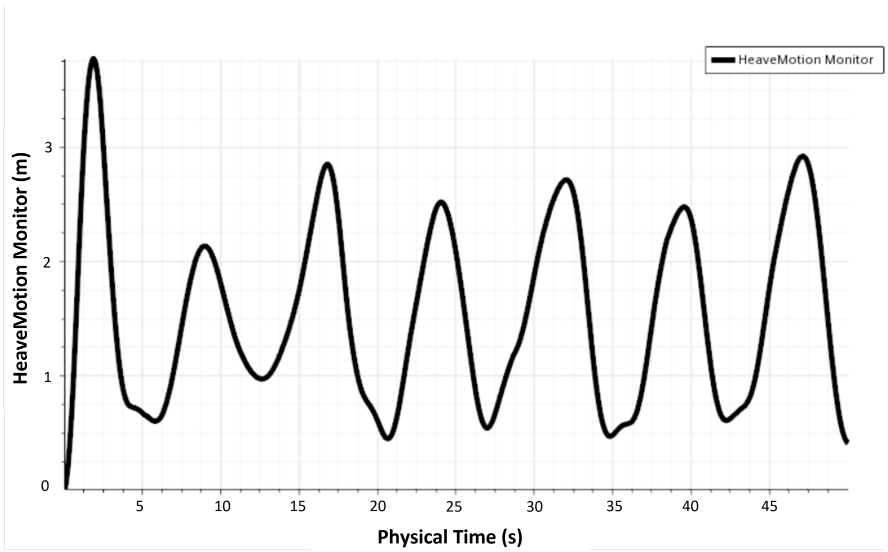

Figure 4.12: Heave plot without damping force at simulation time, t=50 s.

Table 4.4: Without coupling and with coupling simulation parameters

Case	Wave period (s)	Elastic coefficient (N/m)	Damping coefficient (N/s-m)
Without coupling	5	0	0
With coupling		75,000	75,000

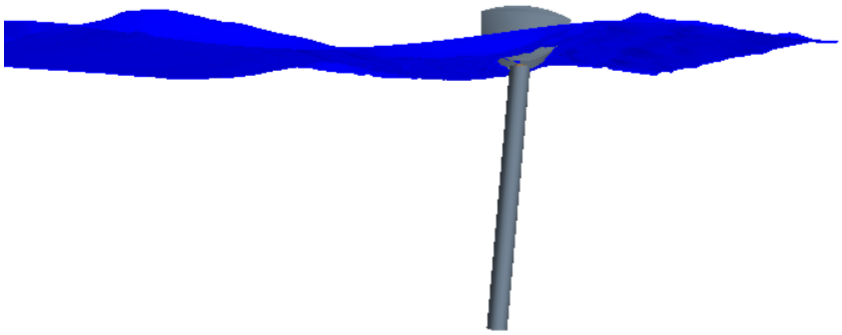

Figure 4.13: Water surface with damping force applied at simulation time, t=50 s.

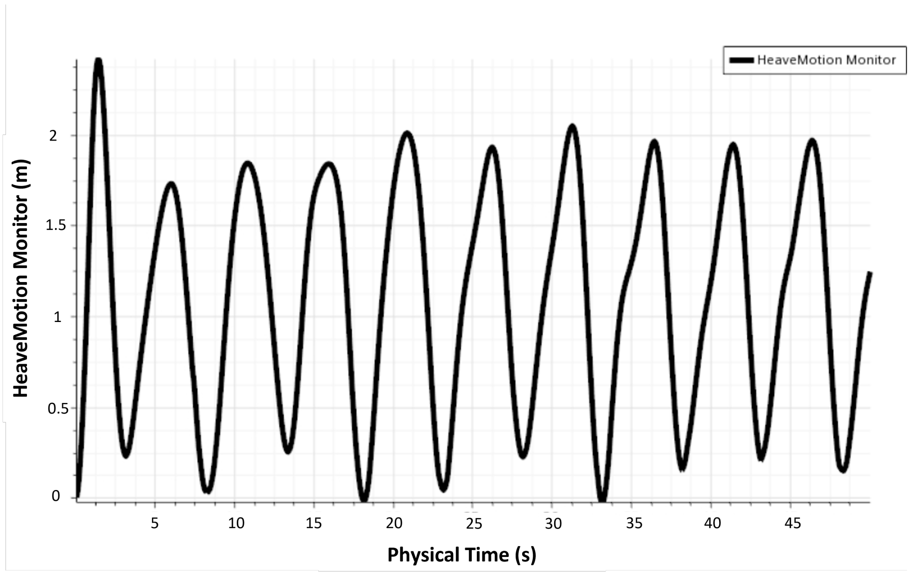

Figure 4.14: Heave plot with damping force applied at simulation time, t=50 s.

4.4.2 Linear spring and Catenary coupling models

Under this section, the two-different coupling models which are most similar in resemblance to the actual mooring lines are included in the simulation setup. First, to begin with the mooring lines in NoviOcean 500 prototype can be seen in Figure 2.6 where they are coupled to the WEC close to the center and in the lower one-third of the geometry. The physical principle of these systems are discussed in the previous chapter 2.5 and can be referred to for deeper understanding.
The Figure 4.15 shows the layout of the linear spring damper and catenary coupling systems. With one end of the system coupled to the mooring point is on the WEC and the other end is defined in the environment. The major difference between the

linear spring and catenary coupling models is in the heave motion characteristic. For the linear spring model a smooth and uniform heave motion curve as seen in Figure 4.14, whereas for the catenary coupling model at the crest of the wave, it can be observed that there is a slightly erratic curve in Figure 4.17.

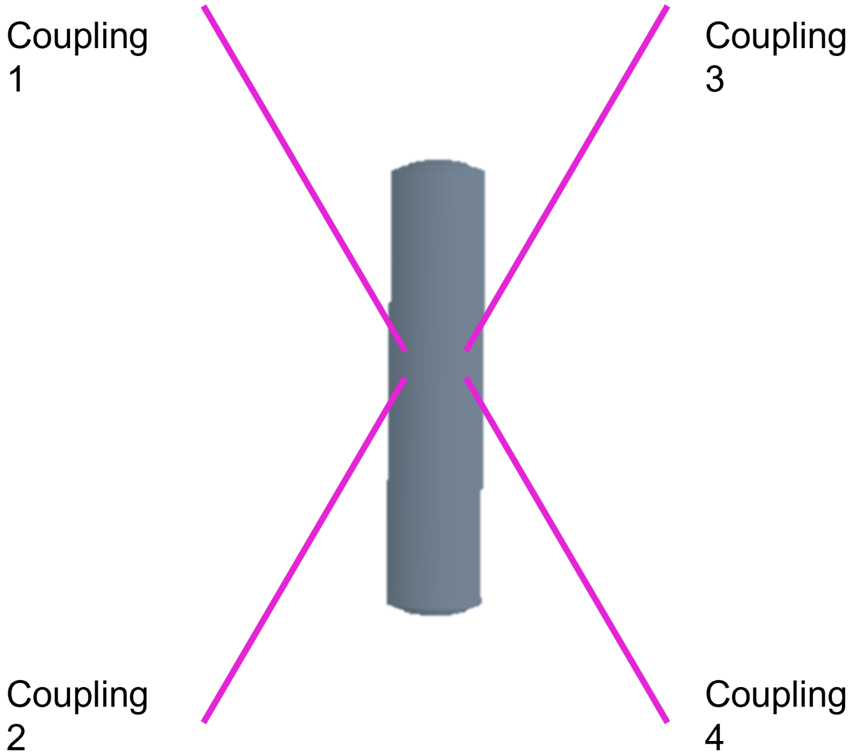

Figure 4.15: Coupling model layout, top view.

The Table 4.5 gives the simulation setup parameters for both the coupling models used in this project. For the catenary system, the mass per unit length, which is the 'linear density' was calculated by assuming a commonly used mooring line material 'polyester' from among other options like polypropylene, polyethylene, polyamide and aramid fibers. Polyester was chosen because of it's high-resistance to UV, it does not lose strength when wet and higher coefficient of friction . The diameter of the mooring line is assumed to be 0.1 m, the density of polyester is approximately 1200 kg/m^3, then the area is computed to be approximately 0.007 m^2. This gives the linear density of the material as approximately 8.4 kg/m, which has been used in the simulation parameters. The relaxation length was assumed to be 5 m for both simulation cases.

Table 4.5: Simulation setup for the different coupling models

Case	**Elastic coefficient/ Stiffness (N/m)**	**Damping coefficient (N/s-m)**	**Mass per unit length (kg/m)**
Linear spring system	75,000	75,000	NA
Catenary system	85,000	NA	8.4

Figure 4.16: Water surface when catenary coupling model is used, at simulation time, t=50 s.

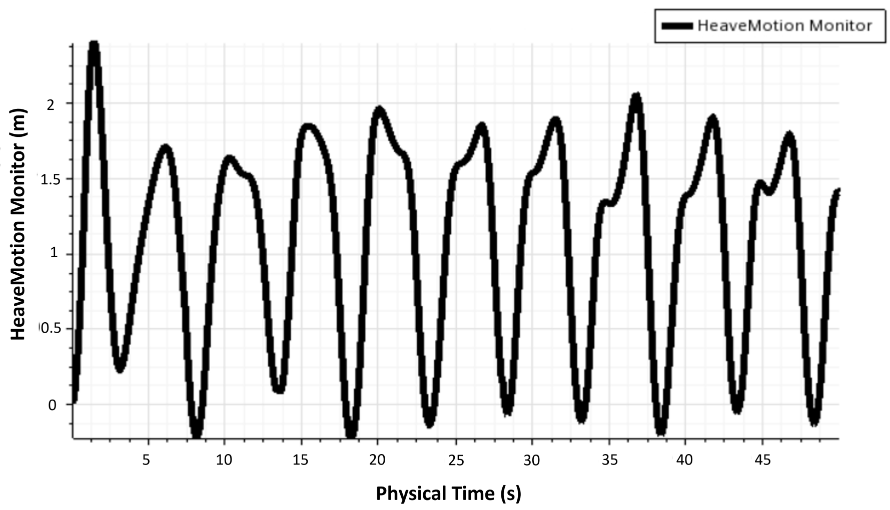

Figure 4.17: Heave plot when catenary coupling model is used, at simulation time, t=50 s.

Further, the mooring length variation during the wave propagation is shown in Figures 4.18 and 4.19. The mooring length for both the catenary and linear spring are set at the same length of 43.05 m, this is actually determined by the end position points and not set manually. Further, the elongation plot shown in the below plots corresponds to the coupling 1 (spring-damper 1), whose position is shown in Figure 4.15. The position of the catenary couplings is also in the same configuration as shown in Figure 4.15. Since, the stiffness, damping coefficients and mass per unit length parameters are the same, the elongation of only one coupling is shown here. As it can be seen in Figures 4.18 and 4.19 the profile of the curves is very similar for both coupling models, the only difference is observed in the spring elongation length for the catenary coupling which is larger than the linear spring coupling model. At the highest peak, the linear spring has a elongation of 0.94 m compared to catenary coupling which has 1.7 m, this is more than a 40% more increase in the elongation when using the latter mentioned coupling model. This could be since the catenary model as discussed in the previous Section 2.5, is a elastic catenary and is modeled as a curve formed by a wire under no tension. This is very close to the physical behaviour of the mooring lines coupled to a WEC.

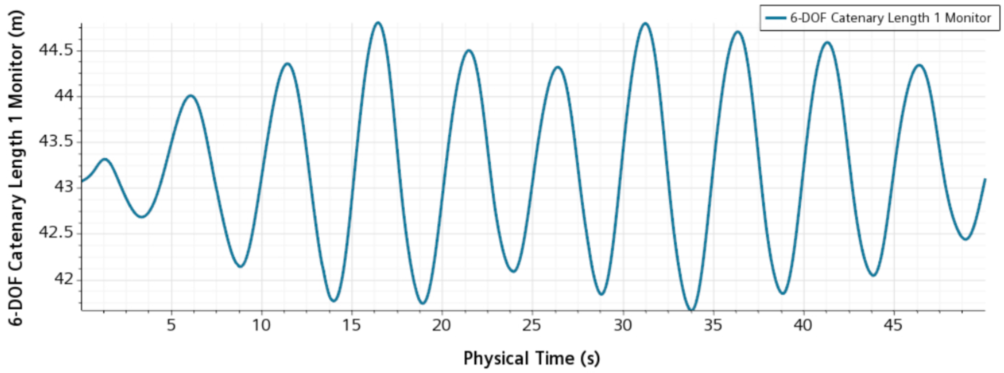

Figure 4.18: Elongation plot of catenary coupling at simulation time, t=50 s.

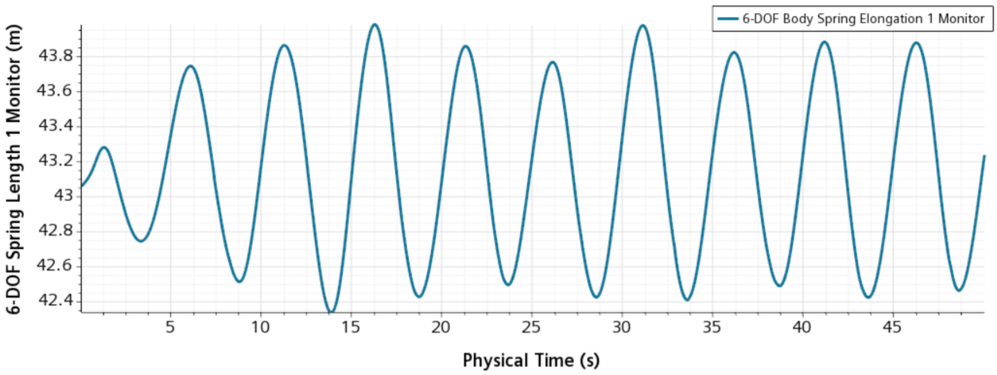

Figure 4.19: Elongation plot of linear spring coupling at simulation time, t=50 s.

Also it is interesting to look at the coupling forces during the wave propagation, as this helps understand better the type of mooring lines and failures, which can aid in the real world testing of NoviOcean 500. The Figures 4.20 and 4.21 show the coupling forces (Newton) acting on the system. Again as mentioned above, the coupling 1, whose position is shown in Figure 4.15 is used to make the comparison. The maximum coupling force observed in Figure 4.21 is 1,731,190 N which is for the linear spring and the maximum force observed at the same point for the catenary coupling is 1,872,900 N, which is around 7.5% more than the linear spring model. These values of coupling forces are very high and this is because of the small relaxation length and the high stiffness value in the spring and catenary coupling. An high stiffness value had to be used in the coupling to keep the WEC stable during the wave propagation.

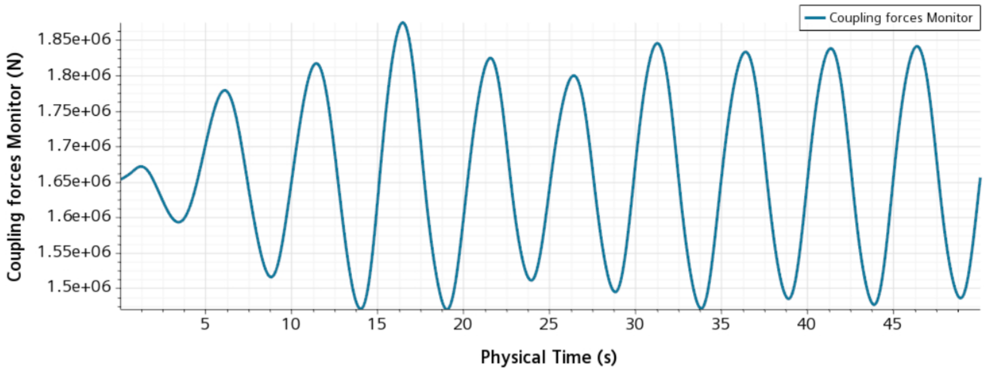

Figure 4.20: Coupling forces, catenary coupling at simulation time, t=50 s.

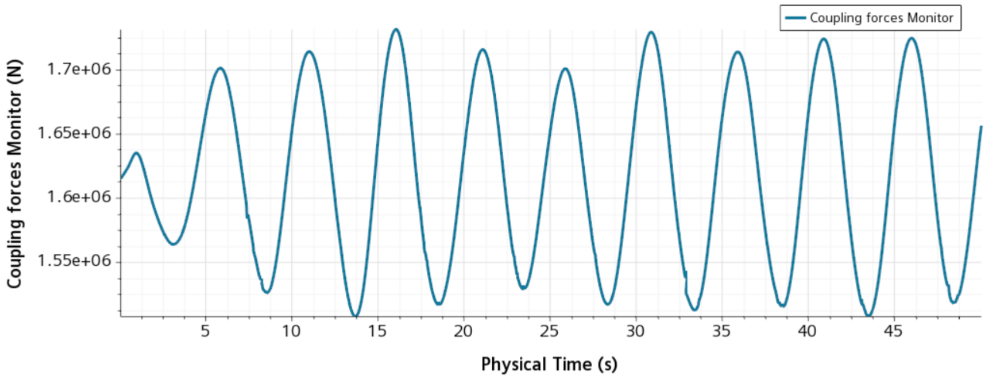

Figure 4.21: Coupling forces, linear spring coupling at simulation time, t=50 s.

4.5 Catenary coupling model with bottom fixed

4.5.1 Simulation setup

In this final section of the results chapter, based on the conclusions drawn from the previous sections, the simulation parameters are setup to simulate the actual configuration of the WEC, shown in Figure 2.7 where the bottom of the hydraulic cylinder is fixed to the sea-floor and this helps with latching with the incoming waves and generating the lift force necessary. So a catenary coupling model is chosen for this simulation, given the more closer resemblance with real mooring line behavior. Further to arrest the motion of the bottom of the hydraulic cylinder, a spring damper system is used which then depicts the damping force applied by a fixed constraint. The same simulation setup parameters as used in Table 4.5 are used for both of the coupling models.

4.5.2 Results

The Figure 4.23 shows the water surface and the heave motion plot for the simulation with the bottom fixed. This can be compared with the simulation results of the catenary coupling model shown in Figure 4.17 with the curve characteristics remaining the same, but the changes are observed in the amplitude of heave motion, because of the damping when the bottom is fixed, we see that the maximum amplitude is 1.237 m which is smaller in comparison to 1.81 m observed without the bottom being damped. Also, the results can be said are more close to physical conditions, since the amplitude of the heave motion is around 1.1-1.2 m as seen in Figure 4.23, which is around 65-70% of the specified wave height of 1.75 m specified in this case. This result is well agreeable with the physical tests in which the heave amplitude corresponds to around 60% of wave height.

Figure 4.22: Water surface with bottom of cylinder fixed at simulation time, t=120 s.

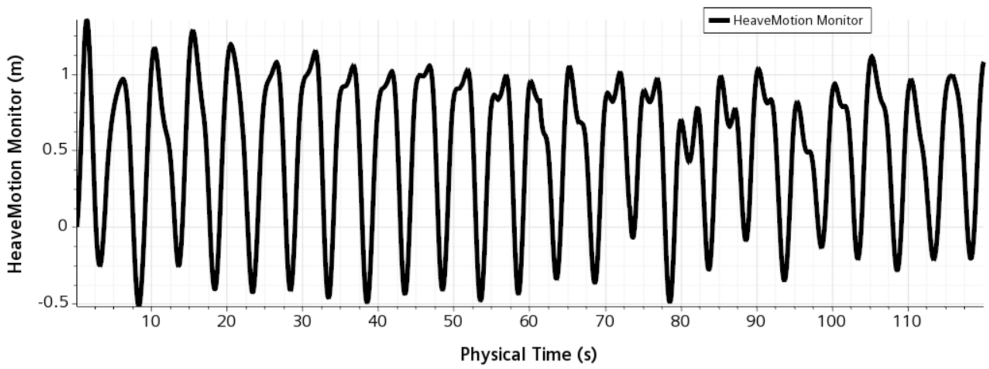

Figure 4.23: Heave motion with bottom of cylinder fixed at simulation time, t=120 s.

The below velocity contours in the wave propagation direction are interesting to discuss, because of how well they illustrate the working of the wave force damping model at the pressure outlet. The region which is 2 times wavelength observed in Figure 4.24 shows how in this region the flow velocity of the propagating wave is arrested and there is no flow reversal, meaning the WEC is not affected by the effects of wave reflection of the boundary. Also, as expected there is flow reversal in the region immediately before and behind the WEC, as seen from Figure 4.25. Also this shows that the kinetic energy $0.5 * m * v^2$ which is a function of velocity, is being harnessed by the WEC effectively in these regions. The wave velocity is found to be maximum at the regions which are the wave troughs, where the wave is accelerating because of gravity.

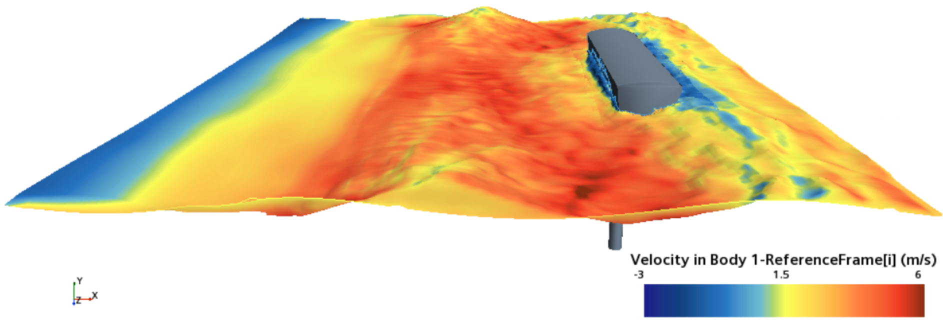

Figure 4.24: Velocity contour, side view.

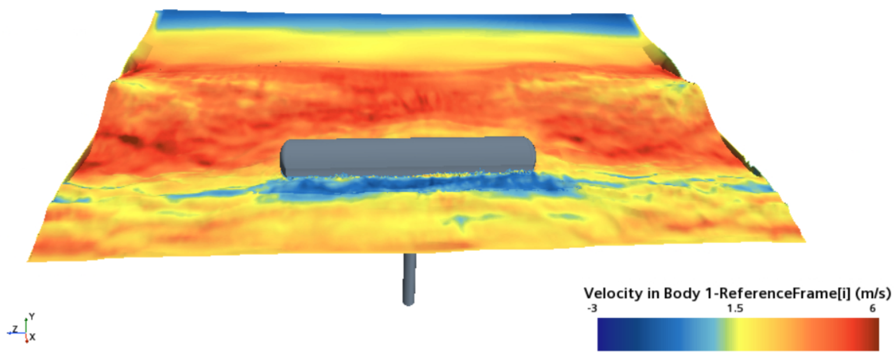

Figure 4.25: Velocity contour, front view.

5
Conclusions

In this thesis work, NoviOcean 500 was studied using the commercial CFD code STAR-CCM+. The focus of this study has been to have a simulation setup that can accurately analyze the various forces acting on the WEC, along with the mooring forces in STAR-CCM+. The study has considered several relevant parameters and simulation settings available in STAR-CCM+ and of importance to the project. These include the various wave generation models, different wavelength, wave periods and different WEC coupling models for mooring lines. The results of these various simulation cases have been discussed and were compared with each other to work towards an simulation setup that can closely capture all the physical effects accurately, which then in a later work can be compared with experimental and test data of NoviOcean 500. It is found that the use of the fifth order Stokes wave model gave results which corresponded well with the regular sea state. The irregular wave model corresponded well with severe sea states, which can be useful to study the survivability of NoviOcean 500 during storms and adverse weather conditions.
It is also proved that, the use of the wave period as wave generation parameter is more accurate than using wavelength, since the wave periods are calculated to be too small when using wavelength as a parameter. Further in the study, the difference in heave motion amplitude with and without coupling models is shown. It can be concluded that, the use of the coupling models dampen the heave amplitude to an extent. Finally, the use of coupling models gave some results like the coupling forces which were not physical and too high and this was concluded to be due to the small relaxation length and high stiffness coefficient values.
Overall, the project provides a simulation model to effectively study and accurately analyze the FSI effects acting on NoviOcean 500 using the commercial code STAR-CCM+.

6
Future work

A few questions which arose during this thesis work, that can be addressed in the future work pertaining to the study of NoviOcean 500. These questions are listed as below:

- The study of mooring forces. In this project, the mooring forces were studied using the simplified systems of coupling available which use a linear theory to resolve the coupling forces acting on the WEC. But the use of dedicated tools like SESAM, which work on non-linear theory, can better help in resolving the mooring forces.
- Since, the WEC's are deployed on-site in a structured setup, similar to wind farms, the effect of wake propagation and wave reflection effects in such a setup, would help in understanding the potential of NoviOcean 500 better.
- Also including more physical parameters like wind speed and current speed in the simulations and studying the change in behaviour of NoviOcean 500, would help predict the performance under various weather conditions and in different ocean currents.

Addressing these questions would further enhance the complete high-fidelity study of NoviOcean 500, taking into account more simulation parameters.

Bibliography

[1] Edenhofer, O., Pichs-Madruga, R., Sokona, Y., Seyboth, K., Matschoss, P., Kadner, S., Zwickel, T., Eickemeier, P., Hansen, G., Schloemer, S., & Stechow, C.V. (2011). Renewable Energy Sources and Climate Change Mitigation. *The Intergovernmental Panel on Climate Change (IPCC)*, Report.

[2] Kempener, R., & Neumann, F. (2014). International Renewable Energy Agency (IRENA). *Wave Energy Technology Brief.* IRENA, Dubai.

[3] NoviOcean. (2020). *Numbers.* https://noviocean.energy/numbers-blue-economy-green-electricity-capex-opex-lcoe-cfd-capacity-factor-commercial-array/

[4] Davidson, L. (2022, March 19). Fluid mechanics, turbulent flow and turbulence modeling.

[5] Sharay, A., & Iglesias, G. (2015, July). Enhancing wave energy competitiveness through co-located wind and wave energy farms. A review on the shadow effect. *Energies.* doi: 10.3390/en8077344

[6] The Liquid grid. (2018). *A technology brief on wave energy converters (WECs) that harvest energy from ocean waves.* `https://theliquidgrid.com/marine-clean-technology/wave-energy-converters/#:~:text=Wave%20energy%20converters%20can%20generally,differential%2C%20and%20rotating%20mass%20devices.`

[7] Vukajlović, N., Katie, V., Milicevic, D., Dumnic, B., & Popadic, B. (2018). Active Control of Induction Generator in Ocean Wave Energy Conversion System. *IEEE 18th International Power Electronics and Motion Control Conference (PEMC),* pp. 324-329. doi: 10.1109/EPEPEMC.2018.8521902

[8] Cui, Y. & Liu, Z. (2014). Effects of Solidity Ratio on Performance of OWC Impulse Turbine. *Advances in Mechanical Engineering.* doi: 10.1155/2014/121373

[9] University of Strathclyde. (2022). *Attenuator (Pelamis - Pelamis Wave Power).* `https://www.esru.strath.ac.uk/EandE/Web_sites/14-15/Wave_Energy/attenuator.html`

[10] Siemens Digital Industries Software. (2021). Simcenter STAR-CCM+ User Guide, version 2021.3. *Siemens.*

[11] Fenton, & John, D. (1985). "A Fifth-Order Stokes Theory for Steady Waves", *Waterway, Port, Coastal and Ocean Eng.* 111 (2), pp. 216-234.

[12] Kraaiennest & CC BY-SA 3.0. (2020). *File:Sine wave amplitude.svg.* `https://commons.wikimedia.org/w/index.php?curid=4038226`

[13] Haun, S., Feurich, R., & Olsen, N.R.B. (2011). Numerical Modeling of Flow Over Trapezoidal Broad-Crested Weir. *Engineering Applications of Computational Fluid Mechanics.* 5. 397-405. doi: 10.1080/19942060.2011.11015381

[14] Tran, T., Krueger, A, Gunawan, B., Alam, M. (2019). Predicting the Dynamic Characteristics of a Fully Submerged Wave Energy Converter Subjected to a Power Take-Off Failure using a High-Fidelity Computational Fluid Dynamics Model. *Paper presented at 13th European Wave and Tidal Energy Conference (EWTEC 2019)*, Naples, Italy.

[15] Windt, C., Davidson, J., Chandar, D.D.J. & Ringwood, J.V. (2020). Evaluation of the overset grid method for control studies of wave energy converters in OpenFOAM numerical wave tanks. *Ocean Eng. Mar. Energy 6*, 55–70. doi: 10.1007/s40722-019-00156-5

[16] Windt, C., Davidson, J., & Ringwood, J.V. (2021). Investigation of Turbulence Modeling for Point-Absorber-Type Wave Energy Converters. *Energies*.14(1):26. doi: 10.3390/en14010026

[17] Devolder, B., Stratigaki, V., Troch, P., & Rauwoens, P. (2018) CFD Simulations of Floating Point Absorber Wave Energy Converter Arrays Subjected to Regular Waves. *Energies.* 11(3):641. doi: 10.3390/en11030641

[18] van Rij, J., Yu, Y.H., McCall, A. & Coe, R.G. (2019). Extreme Load Computational Fluid Dynamics Analysis and Verification for a Multibody Wave Energy Converter. *ASME 2019 38th International Conference on Ocean, Offshore and Arctic Engineering.* doi: 10.1115/OMAE2019-96397

[19] Kisacik, D., Stratigaki, V., Wu, M., Cappietti, L., Simonetti, I., Troch, P., Crespo, A., Altomare, C., Domínguez, J., Hall, M., Gómez-Gesteira, M., Canelas, R., & Stansby, P.K. (2020). Efficiency and Survivability of a Floating Oscillating Water Column Wave Energy Converter Moored to the Seabed: An Overview of the EsflOWC MaRINET2 Database. *Water* 12. 992. doi: 10.3390/w12040992

DEPARTMENT OF MECHANICS AND MARITIME SCIENCES
CHALMERS UNIVERSITY OF TECHNOLOGY
Gothenburg, Sweden
www.chalmers.se

CHALMERS
UNIVERSITY OF TECHNOLOGY